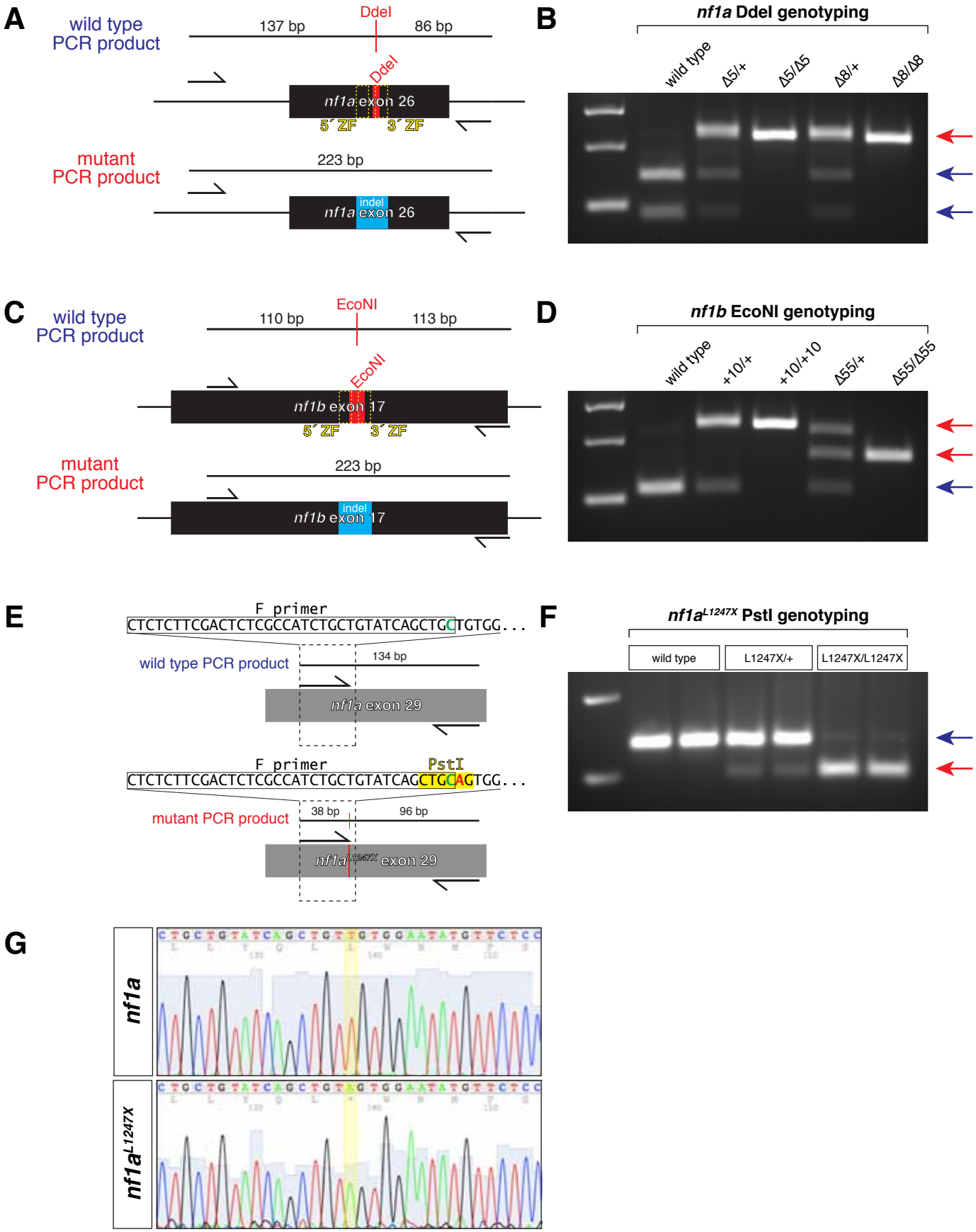

Fig. S1. Genotyping strategies for identification of nf1 mutant alleles.
(A,B) Schematic diagram of PCR products generated from wild type and ZFN-induced mutant *nf1a* alleles (A). The indels (A, blue box) in the Δ8 and Δ5 *nf1a* alleles lead to loss of a native DdeI site, allowing for allelic discrimination by gel electrophoresis of DdeI digested PCR products (B, red arrow, mutant band; blue arrows, wild type bands). (C,D) Schematic diagram of PCR products generated from wild type and ZFN-induced mutant *nf1b* alleles (C). The indels (C, blue box) in the +10 and Δ55 *nf1b* alleles lead to loss of a native EcoNI site, allowing for allelic discrimination by gel electrophoresis of EcoNI digested PCR products (D, red arrows, mutant bands; blue arrow, co-migrating wild type bands). (E,F) Schematic diagram of PCR products generated from wild type and TILLING-induced *nf1a*^{L1247X} alleles (E). The forward primer (F primer) contains a 1 base pair mismatch with the native *nf1a* exon 29 sequence so as to create a PstI restriction site in the mutant, which harbors a T to A nonsense mutation, allowing for allelic discrimination by gel electrophoresis of PstI digested PCR products (F, red arrow, mutant band; blue arrow, wild type band). (G) Sequencing chromatograms from wild type and *nf1a*$^{L1247X/L1247X}$ animals (TILLING-induced mutation highlighted).

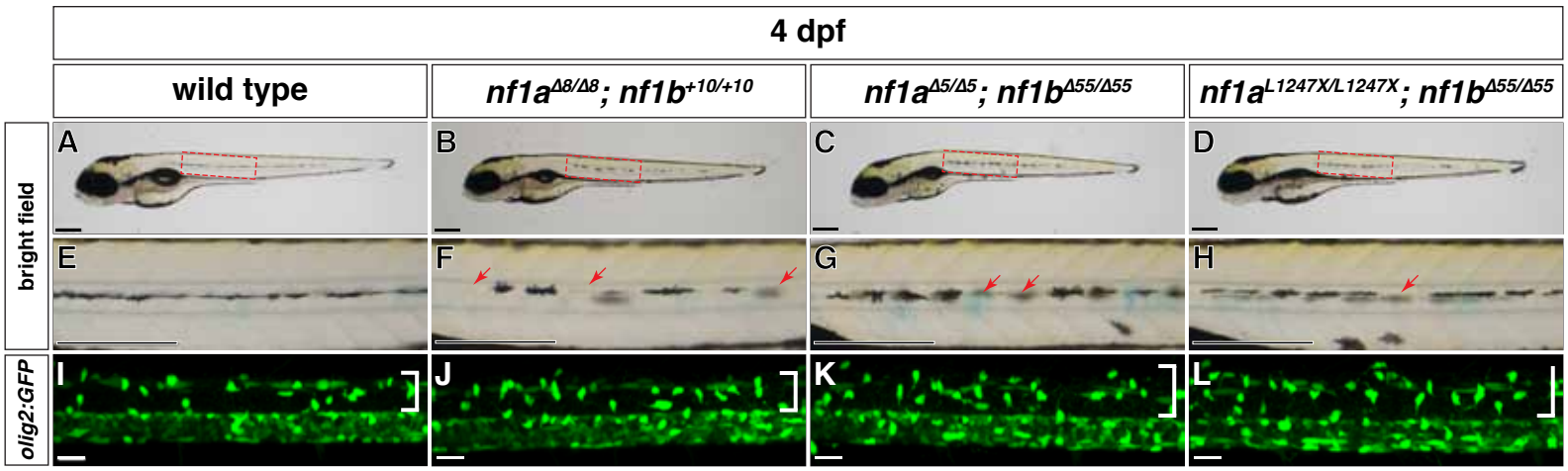

Fig. S2. *nf1*-null mutants with different allelic combinations of *nf1a* and *nf1b* are phenotypically identical. (A-H) Lateral view of wild type (A,E,I), *nf1a*$^{\Delta 8/\Delta 8}$; *nf1b*$^{+10/+10}$ (B,F,J), *nf1a*$^{\Delta 5/\Delta 5}$; *nf1b*$^{\Delta 55/\Delta 55}$ (C,G,K), and *nf1a*$^{L1247X/L1247X}$; *nf1b*$^{+10/+10}$ larvae (D,F,L) at 4 dpf. (E-H) Magnified views of the boxed region in A-D demonstrating absence of melanophores along the lateral line (arrows) in different allelic combinations of *nf1a*; *nf1b* double homozygous mutant alleles. Scale bars: 300 μm. (I-L) Confocal images of spinal cords in Tg(*olig2:GFP*) larvae harboring different allelic combinations of *nf1a*; *nf1b* homozygous mutant alleles at 4 dpf. OPC hyperplasia (brackets) is observed in all three allelic combinations of *nf1a*; *nf1b* double homozygous mutant alleles. Scale bars: 300 μm.

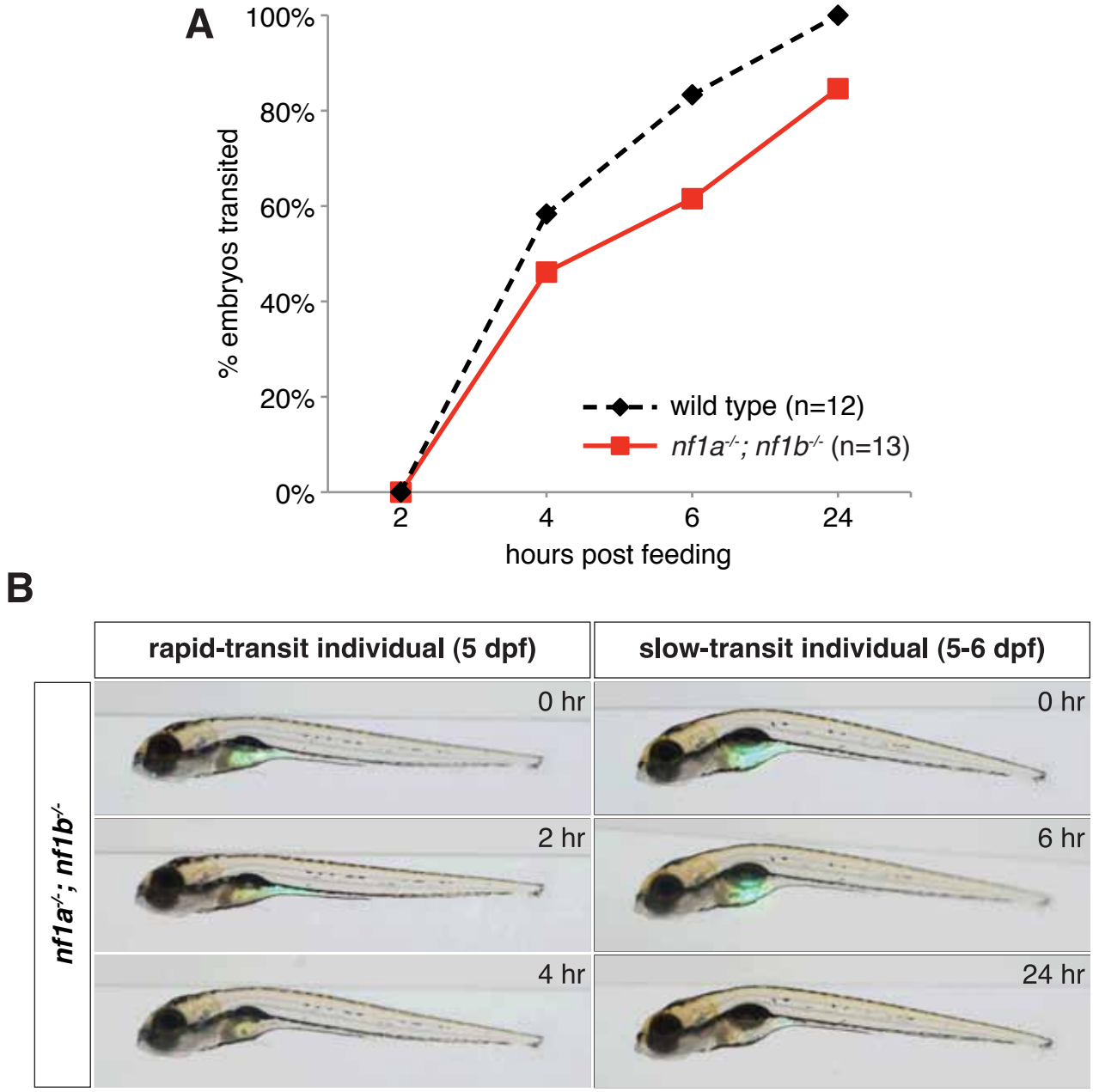

Fig. S3. Loss of *nf1a* and *nf1b* does not affect food consumption or transit.
(A) Graph depicting intestinal transit time for 5 dpf wild type (black line) and *nf1a*$^{-/-}$; *nf1b*$^{-/-}$ (red line) larvae following a 1 hour feeding of paramecia and fluorescent microspheres. Transit was considered to be complete when fluorescent microspheres were no longer detected along the intestinal tract by fluorescent microscopy. (B) Representative overlays of bright field and fluorescent images from 5-6 dpf *nf1a*$^{-/-}$; *nf1b*$^{-/-}$ larvae exhibiting rapid- or slow-transit.

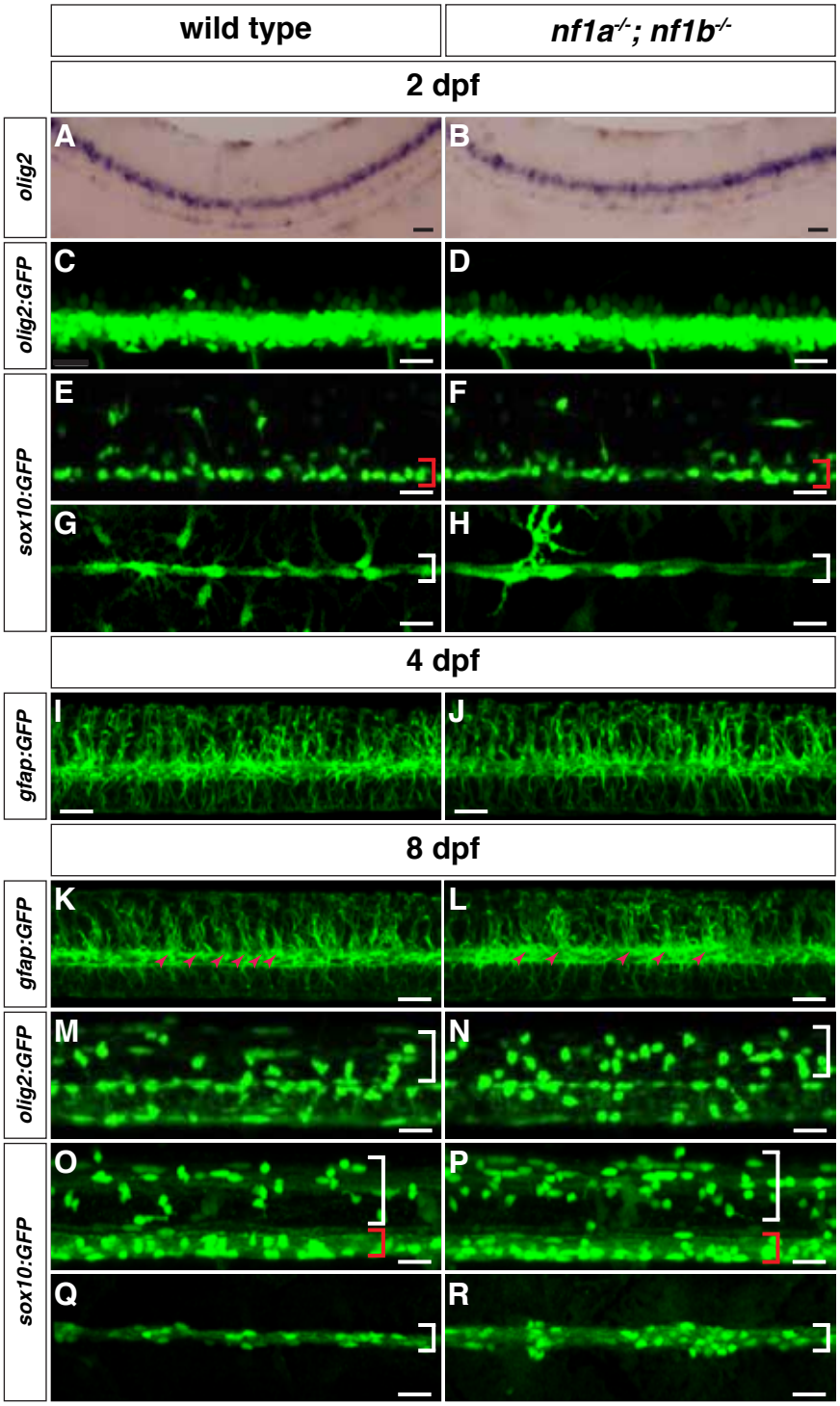

Fig. S4. Analysis of *nf1a*/*nf1b* mutant OPCs and Schwann cells at 2 dpf and radial glia at 4 dpf appear normal with defects appreciated in all three populations at 8 dpf.
(A,B) Whole-mount in situ hybridization for expression of endogenous *olig2* in wild type (A) and *nf1a*$^{-/-}$; *nf1b*$^{-/-}$ (B) larvae at 2 dpf. Scale bars: 20 μm. (C,D) Spinal cord of wild type; Tg(*olig2:GFP*) (C) and *nf1a*$^{-/-}$; *nf1b*$^{-/-}$; Tg(*olig2:GFP*) (D) larvae at 2 dpf. Scale bars: 20 μm. (E,F) Spinal cord of wild type; Tg(*sox10:GFP*) (E) and *nf1a*$^{-/-}$; *nf1b*$^{-/-}$; Tg(*sox10:GFP*) (F) larvae at 2 dpf. Brackets indicate ventrally positioned *sox10*:GFP-positive OPCs. Scale bars: 20 μm. (G,H) PLLn of wild type; Tg(*sox10:GFP*) (G) and *nf1a*$^{-/-}$; *nf1b*$^{-/-}$; Tg(*sox10:GFP*) (H) larvae at 2 dpf. Brackets indicate *sox10*:GFP-positive Schwann cells associated with the PLLn. Scale bars: 20 μm. (I,J) Spinal cord of wild type; Tg(*gfap:GFP*) (I) and *nf1a*$^{-/-}$; *nf1b*$^{-/-}$; Tg(*gfap:GFP*) (J) larvae at 4 dpf. Scale bars: 20 μm. (K,L) Spinal cord of wild type; Tg(*gfap:GFP*) (K) and *nf1a*$^{-/-}$; *nf1b*$^{-/-}$; Tg(*gfap:GFP*) (L) larvae at 8 dpf. Arrowheads depict the normal segmental expression of GFP in wild type larvae (K) that is absent in *nf1a*$^{-/-}$; *nf1b*$^{-/-}$ larvae (L). Scale bars: 20 μm. (M,N) Spinal cord of wild type; Tg(*olig2:GFP*) (M) and *nf1a*$^{-/-}$; *nf1b*$^{-/-}$; Tg(*olig2:GFP*) (N) larvae at 8 dpf. Brackets indicate dorsally positioned *olig2*:GFP-positive OPCs. Scale bars: 20 μm. (O,P) Spinal cord of wild type; Tg(*sox10:GFP*) (O) and *nf1a*$^{-/-}$; *nf1b*$^{-/-}$; Tg(*sox10:GFP*) (P) larvae at 8 dpf. White and red brackets indicate dorsally and ventrally positioned *sox10*:GFP-positive OPCs, respectively. Scale bars: 20 μm. (Q,R) PLLn of wild type; Tg(*sox10:GFP*) (Q) and *nf1a*$^{-/-}$; *nf1b*$^{-/-}$; Tg(*sox10:GFP*) (R) larvae at 8 dpf. Brackets indicate *sox10*:GFP-positive Schwann cells associated with the PLLn. Scale bars: 20 μm.

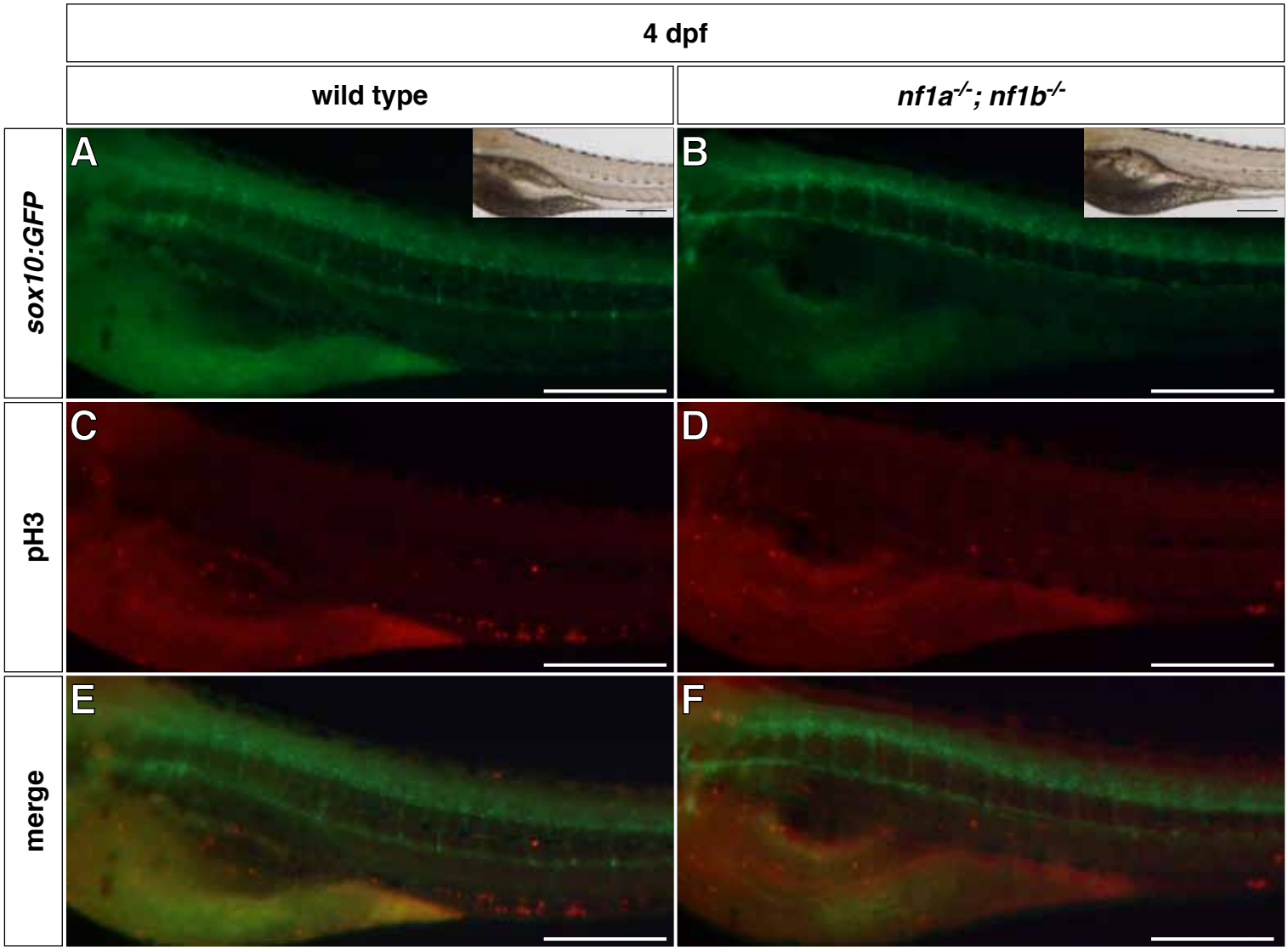

Fig. S5. Increase in posterior lateral line nerve (PLLn) Schwann cell numbers observed in *nf1a*$^{-/-}$; *nf1b*$^{-/-}$ larvae at 4 dpf is not due to increased proliferation.

(A-F) Representative images of transgenic *sox10:GFP* expressing wild type (A,C,E, *n*=13) and *nf1a*$^{-/-}$; *nf1b*$^{-/-}$ (B,D,F, *n*=7) larvae. No increase in phospho-histone H3 (pH3) staining is apparent at 4 dpf in PLLn Schwann cells of *nf1* mutants (D,F) when compared with wild type controls (C,E). Scale bars: 50 μm.

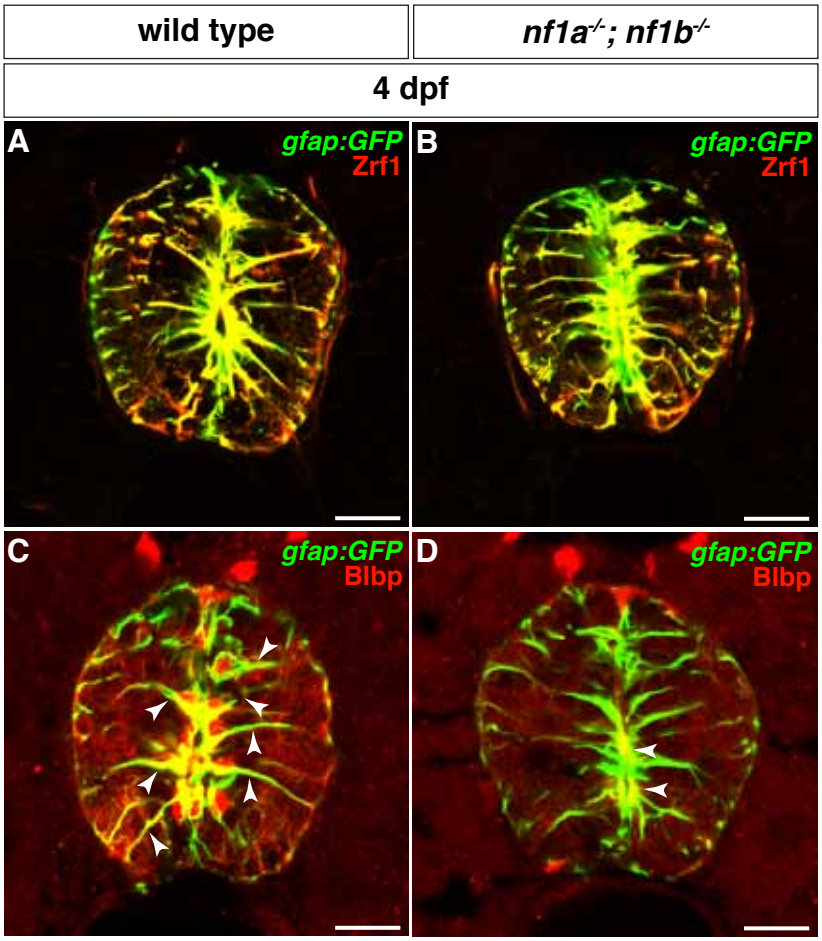

Fig. S6. Radial glia of *nf1a*$^{-/-}$; *nf1b*$^{-/-}$ larvae express reduced amounts of brain lipid binding protein (Blbp). (A,B) Radial glia in transverse sections through the spinal cord of wild type; Tg(*gfap:GFP*) (A) and *nf1a*$^{-/-}$; *nf1b*$^{-/-}$; Tg(*gfap:GFP*) (B) larvae at 4 dpf are marked by expression of the *gfap*:GFP transgene (green) and the Zrf1 antibody (red). (C,D) Radial glia (green) in transverse sections through the spinal cord of *nf1a*$^{-/-}$; *nf1b*$^{-/-}$; Tg(*gfap:GFP*) larvae (D) demonstrate decreased Blbp expression (red), as identified by colocalization (yellow, arrowheads), when compared with wild type; Tg(*gfap:GFP*) larvae (C) at 4 dpf. Scale bars: 20 μm.

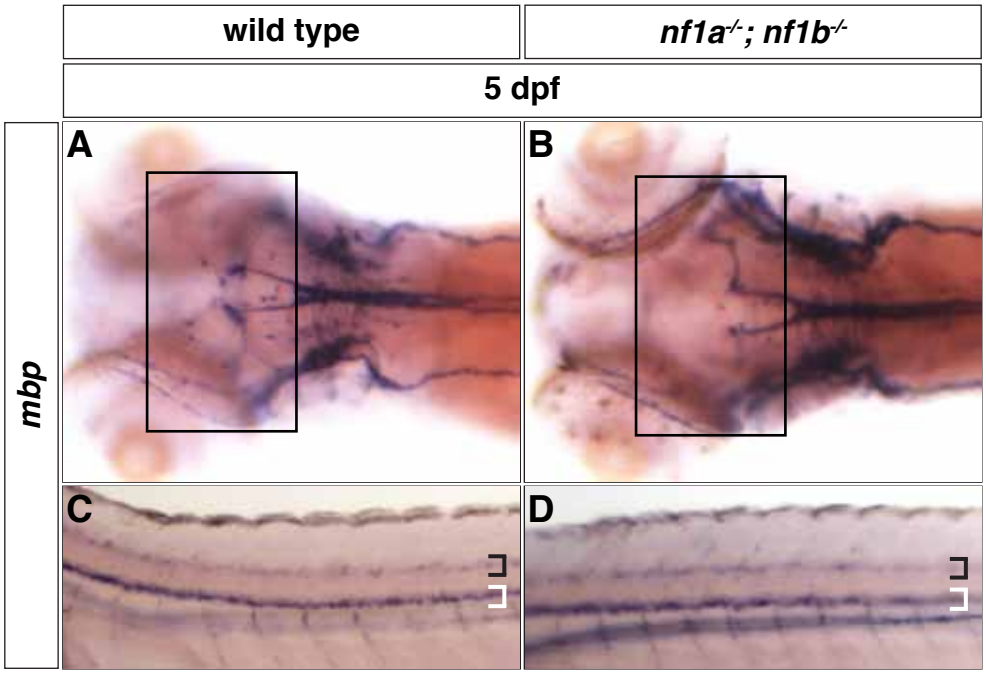

Fig. S7. Expression of *mbp* in the brain and spinal cord of *nf1a*$^{-/-}$; *nf1b*$^{-/-}$ larvae appears normal.
(A,B) No difference in *mbp* expression is appreciated in the midbrain and hindbrain regions (A,B, boxes) as well as along the dorsal (black brackets) and ventral (white brackets) spinal cord of *nf1a*$^{-/-}$; *nf1b*$^{-/-}$ larvae (B,D) when compared to wild type larvae (A,C) by whole mount in situ hybridization at 5 dpf.

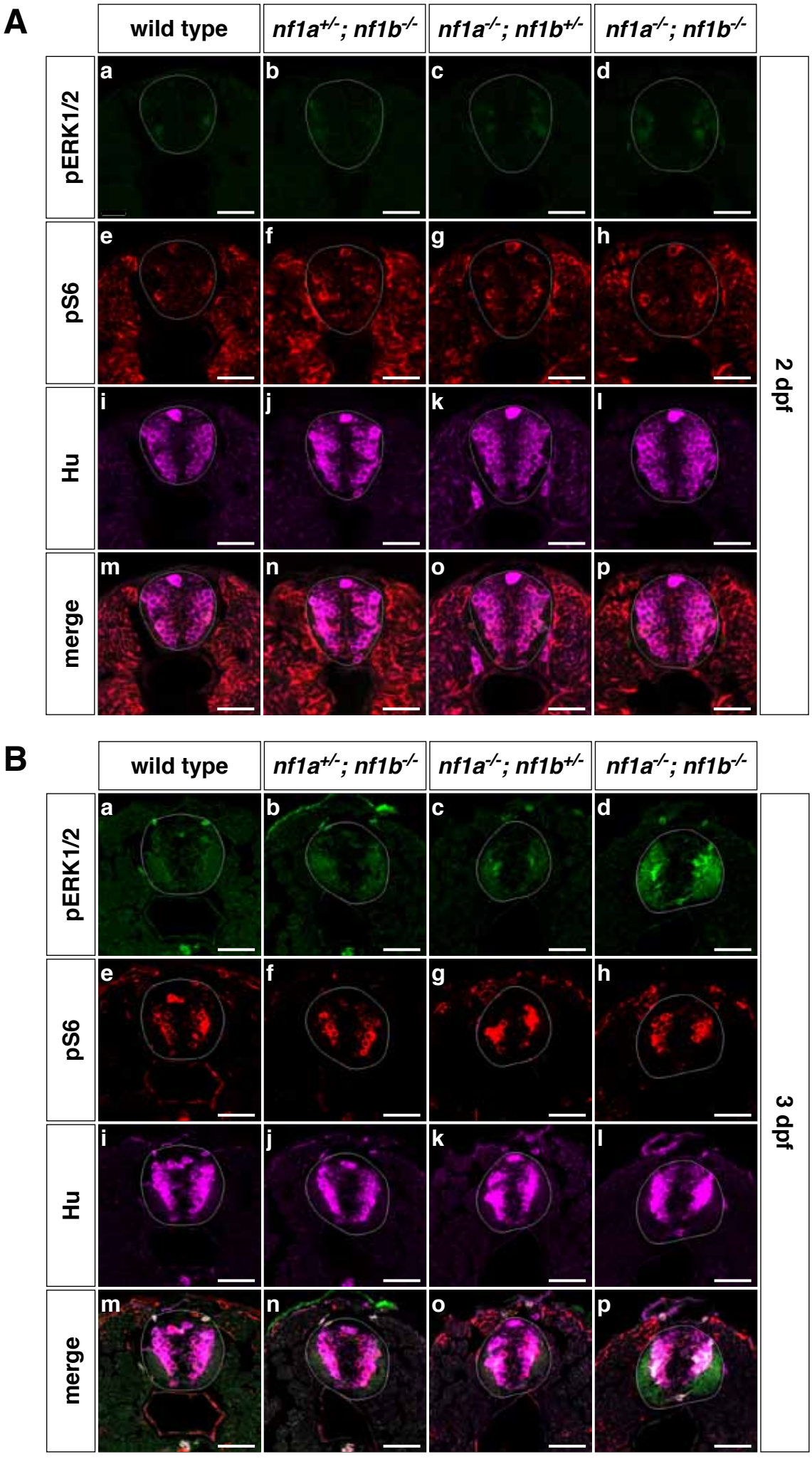

Fig. S8. Increased ERK1/2 phosphorylation is appreciated in the spinal cords of *nf1a*$^{-/-}$; *nf1b*$^{-/-}$ larvae by 3 dpf. Immunohistochemical analysis of transverse sections through the spinal cord of 2 dpf *nf1a*$^{-/-}$; *nf1b*$^{-/-}$ larvae (Ad,Ah,Al,Ap) demonstrates no appreciable differences in pERK1/2 (green) or pS6 staining (red) when compared with *nf1a*$^{+/-}$; *nf1b*$^{-/-}$ (Ab,Af,Aj,An), *nf1a*$^{-/-}$; *nf1b*$^{+/-}$ (Ac,Ag,Ak,Ao), or wild type (Aa,Ae,Ai,Am) larvae. At 3 dpf, however, increased pERK1/2 signal is noted in *nf1a*$^{-/-}$; *nf1b*$^{-/-}$ larvae (Bd,Bp) when compared with *nf1a*$^{+/-}$; *nf1b*$^{-/-}$ (Bb,Bn), *nf1a*$^{-/-}$; *nf1b*$^{+/-}$ (Bc,Bo), or wild type (Ba,Bm) larvae, with no differences noted in levels of pS6 (Be-Bh). Activated ERK1/2 signaling is most prominent in spinal cord neurons, as identified by colocalization (white) with HuC/D expression (magenta) (Bl,Bp). Scale bars: 20 μm.

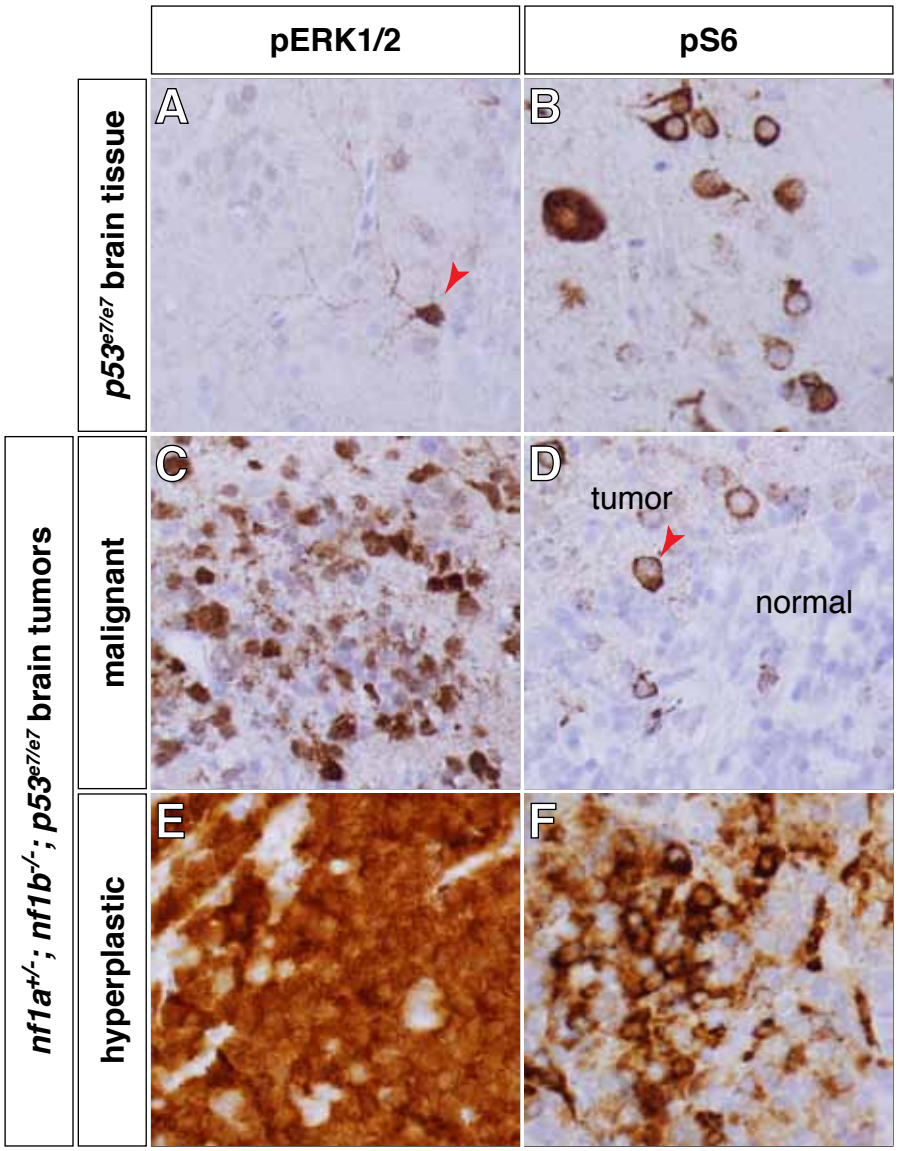

Fig. S9. *nf1a*$^{+/-}$*; nf1b*$^{-/-}$ *;p53*$^{e7/e7}$ brain tumors demonstrate hyperactivation of ERK and mTOR pathways. (A-F) Immunohistochemical analysis of pERK1/2 and pS6 in *p53*$^{e7/e7}$ brain tissue (A,B, red arrow labels normal neuron) as well as *nf1a*$^{+/-}$*; nf1b*$^{-/-}$; *p53*$^{e7/e7}$ brain tumors demonstrating a predominantly malignant (C,D) or hyperproliferative (E,F) phenotype. The more malignant and infiltrative *nf1a*$^{+/-}$*; nf1b*$^{-/-}$; *p53*$^{e7/e7}$ brain tumor demonstrates increased pERK1/2 staining (C), with normal levels of pS6 (D, red arrow labels normal neuron) when compared with similarly stained *p53*$^{e7/e7}$ brain tissue (A,B). The majority of tumor cells in the more hyperplastic *nf1a*$^{+/-}$*; nf1b*$^{-/-}$; *p53*$^{e7/e7}$ brain tumor show staining for pERK1/2 (E) along with heterogeneously increased pS6 (F).

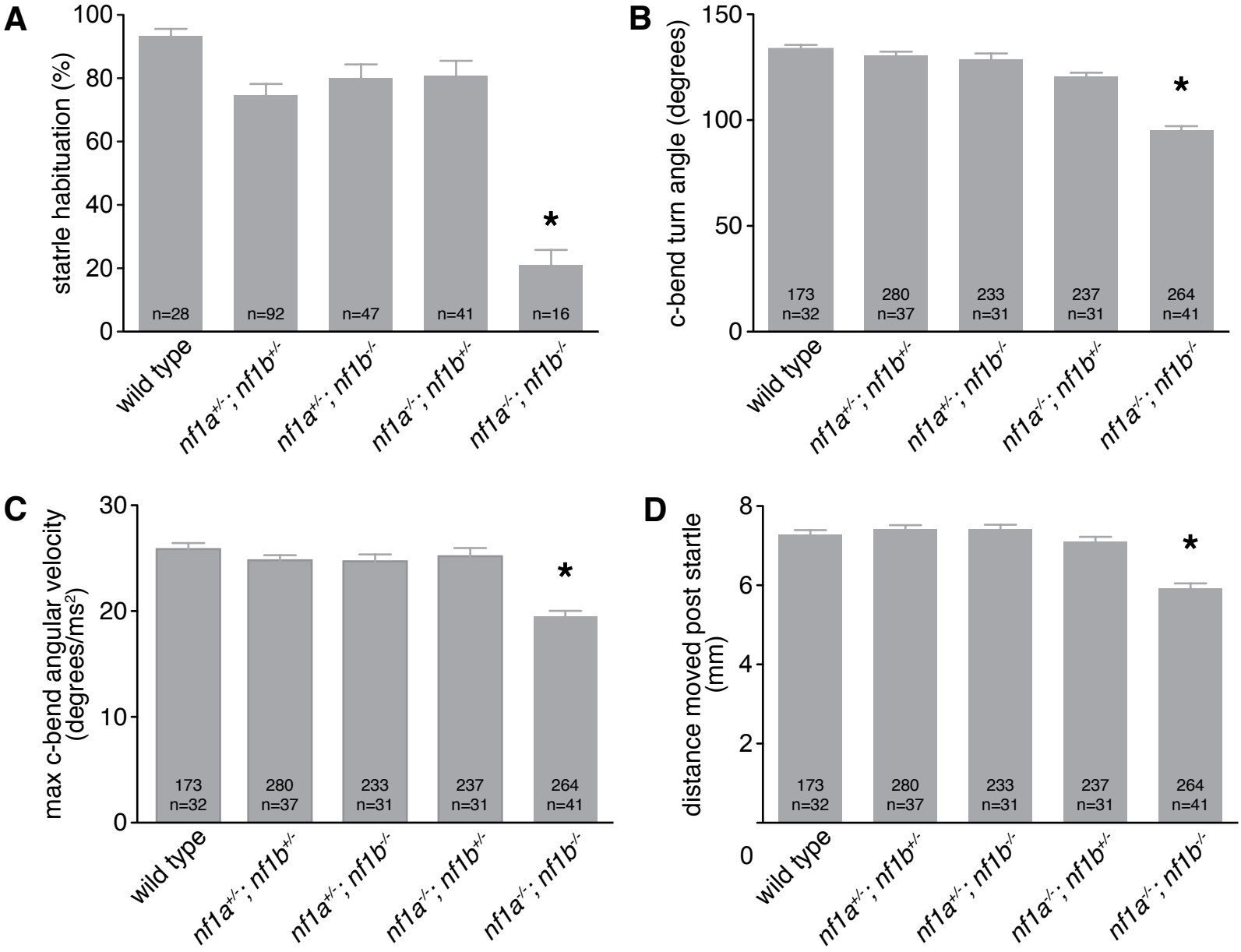

Fig. S10. *nf1a*/*nf1b* mutants exhibit acoustic startle C-start behavioral deficits.
(A) Mean degree of short-term SLC habituation is reduced in 5 dpf *nf1a*$^{-/-}$; *nf1b*$^{-/-}$ larvae. (B-C) Measurement of mean head turning angle (B) and mean maximum angular velocity (C) of initial C-bend following delivery of acoustic stimulus demonstrates a significant reduction of both behavioral measures in 5 dpf *nf1a*$^{-/-}$; *nf1b*$^{-/-}$ larvae. (D) Mean distance traveled over 90 milliseconds following delivery of acoustic stimulus, as a result of short latency C-start behavioral response, is also significantly reduced in 5 dpf *nf1a*$^{-/-}$; *nf1b*$^{-/-}$ larvae. The total number of short latency C-bends and number of larvae tested per genotype appear at the base of each bar graph (*P<0.001).

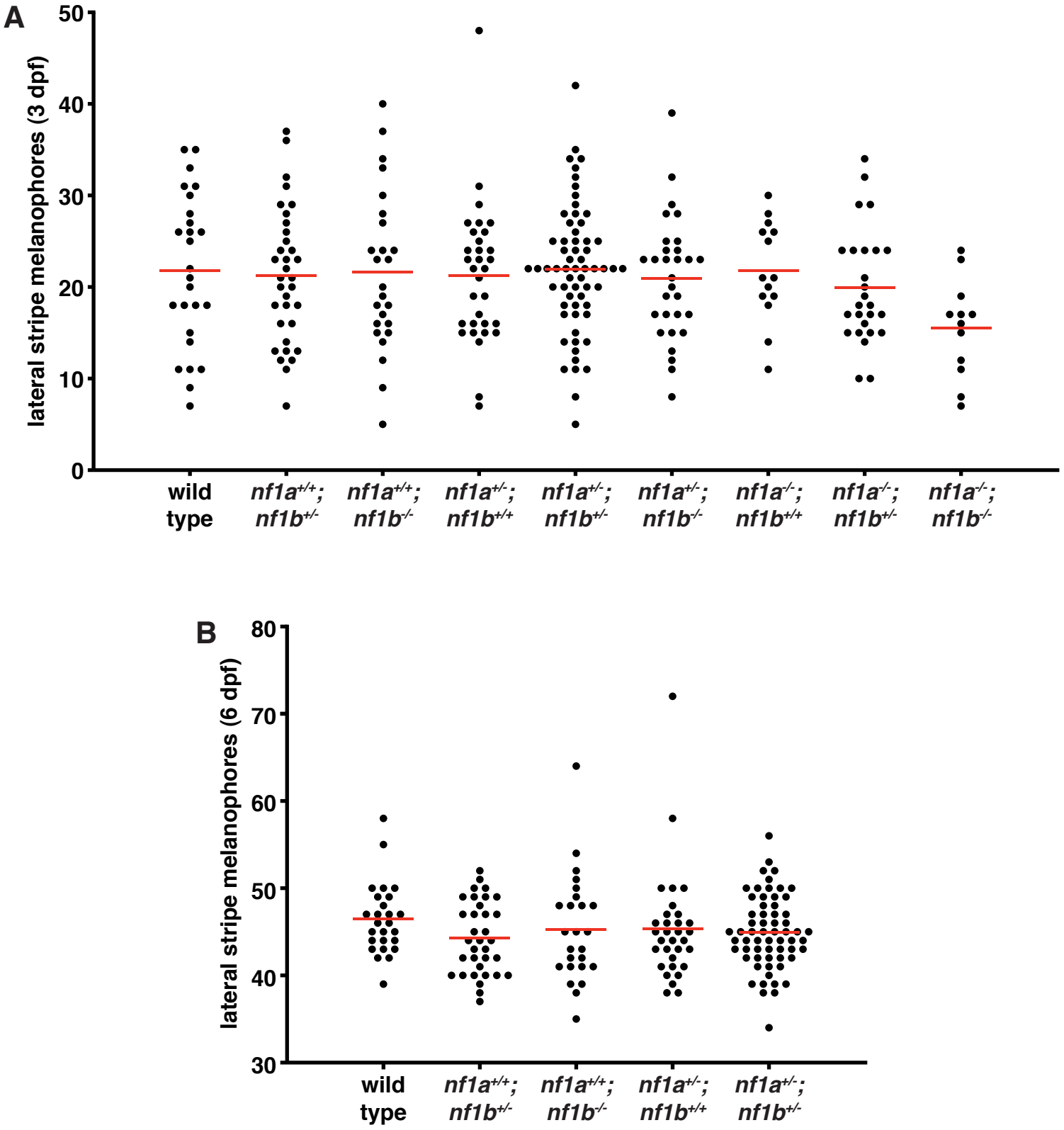

Fig. S11. Quantification of lateral stripe melanophores in wild type and *nf1a*/*nf1b* mutant larvae at 3 and 6 dpf.

(A) Quantification of lateral stripe melanophores from wild type (*n*=26), *nf1a*$^{+/+}$; *nf1b*$^{+/-}$ (*n*=34), *nf1a*$^{+/+}$; *nf1b*$^{-/-}$ (*n*=25), *nf1a*$^{+/-}$; *nf1b*$^{+/+}$ (*n*=32), *nf1a*$^{+/-}$; *nf1b*$^{+/-}$ (*n*=62), *nf1a*$^{+/-}$; *nf1b*$^{-/-}$ (*n*=30), *nf1a*$^{-/-}$; *nf1b*$^{+/+}$ (*n*=14), *nf1a*$^{-/-}$; *nf1b*$^{+/-}$ (*n*=26), and *nf1a*$^{-/-}$; *nf1b*$^{-/-}$ (*n*=12) larvae at 3 dpf. Each point represents the number of lateral stripe melanophores in an individual embryo and red lines indicate mean values. (B) Quantification of lateral stripe melanophores from wild type (*n*=26; same as displayed in Fig. 8), *nf1a*$^{+/+}$; *nf1b*$^{+/-}$ (*n*=34), *nf1a*$^{+/+}$; *nf1b*$^{-/-}$ (*n*=25), *nf1a*$^{+/-}$; *nf1b*$^{+/+}$ (*n*=32), and *nf1a*$^{+/-}$; *nf1b*$^{+/-}$ (*n*=62) larvae at 6 dpf. Each point represents the number of lateral stripe melanophores in an individual embryo and red lines indicate mean values.

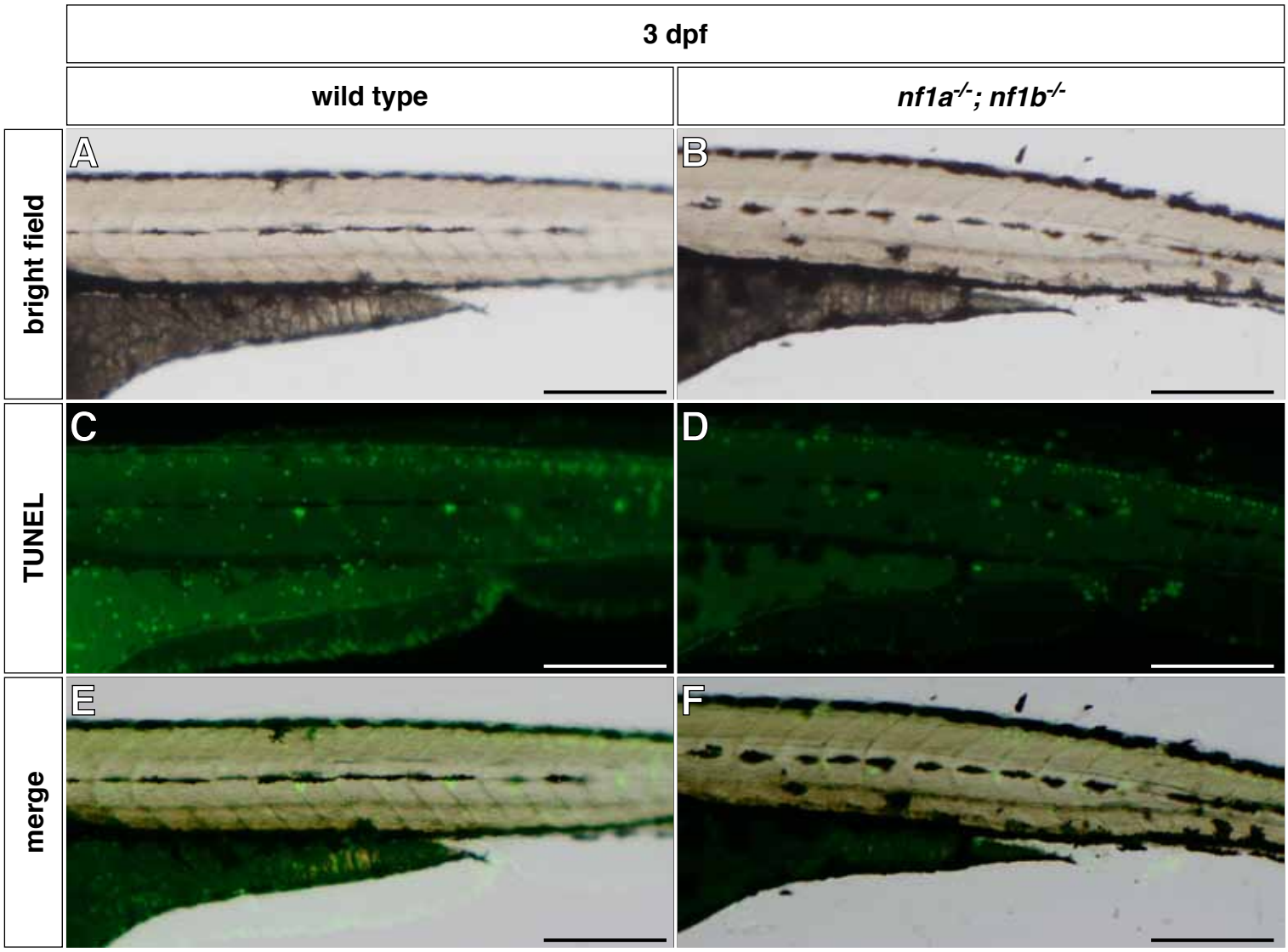

Fig. S12. Melanized embryonic/ontogenetic and unmelanized regeneration and metamorphic melanophores do not demonstrate increased apoptosis at 3 dpf in *nf1a*$^{-/-}$; *nf1b*$^{-/-}$ larvae.
(A-F) Representative images of melanized embryonic/ontogenetic melanophores along the lateral stripe visualized at 3 dpf in wild type (A,C,E) and *nf1a*$^{-/-}$; *nf1b*$^{-/-}$ mutant (B,D,F) larvae. No difference in apoptotic cells was noted (68.1±11 cells/larva, n=12 wild type versus 63.8±8.5, n=12 mutants; P=0.27). No melanized embryonic/ontogenetic cells are noted to be TUNEL-positive in either genotype (C,D), with similar numbers of TUNEL-positive cells appearing in the region where unmelanized regeneration and metamorphic melanophores would be located at this time point (C-F). Scale bars: 50 μm.

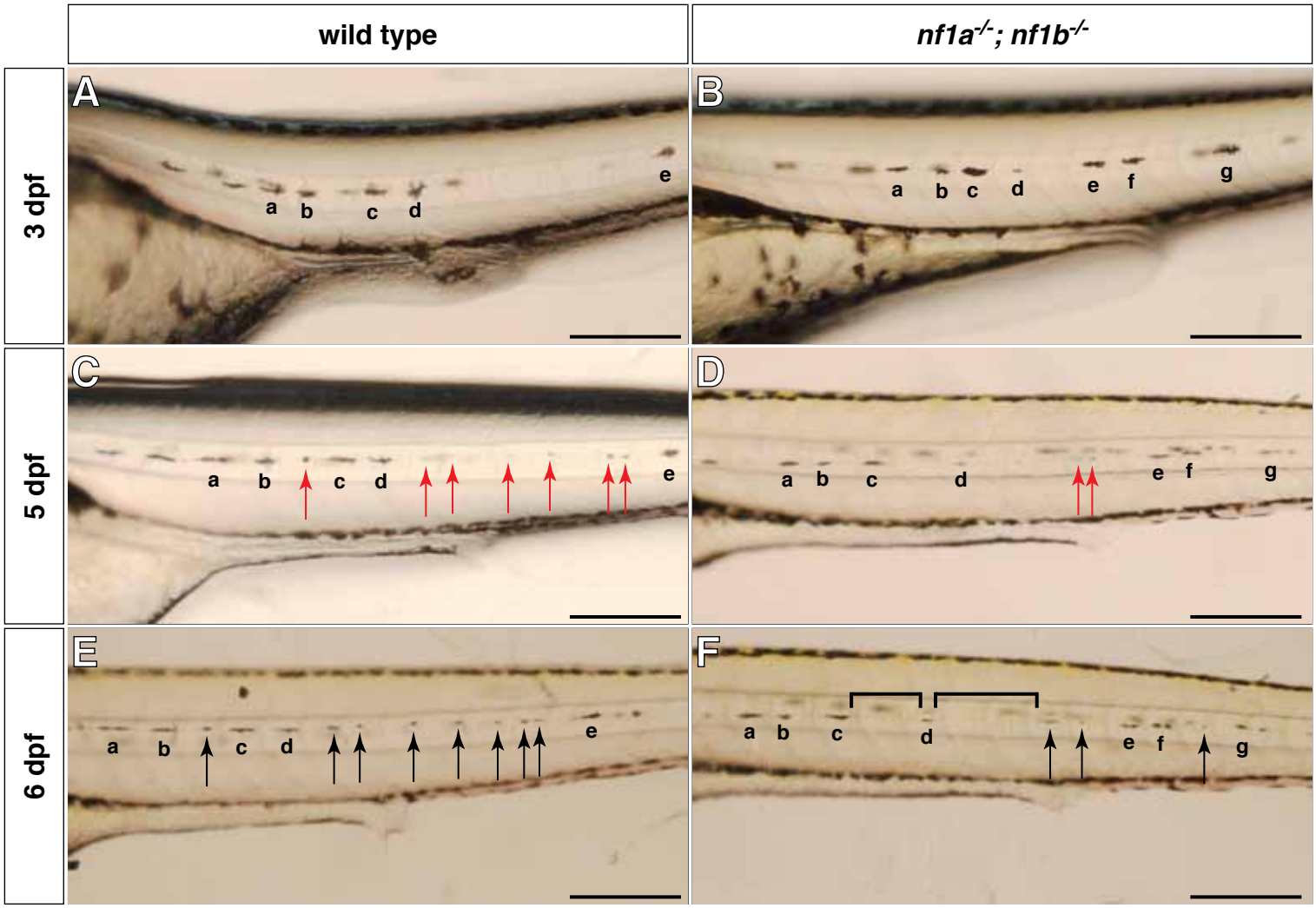

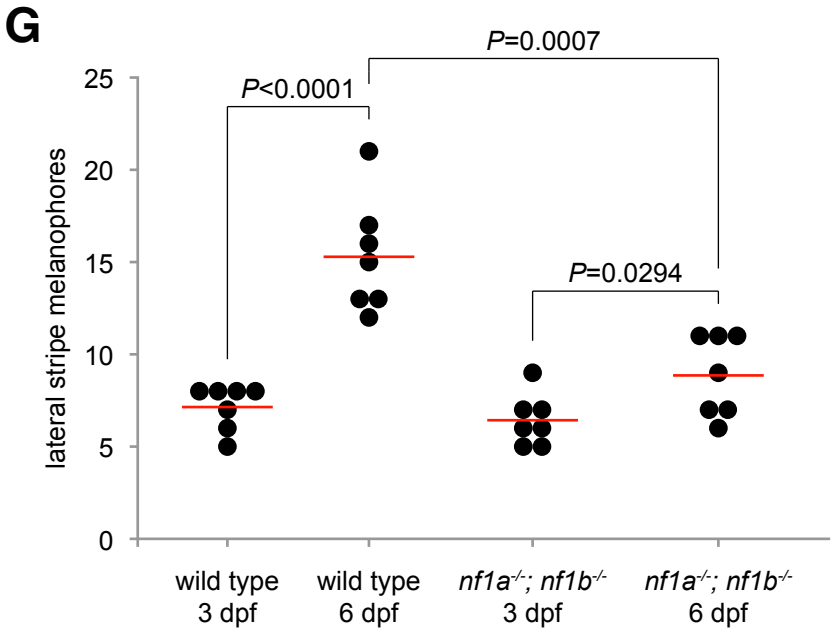

Fig. S13. Gaps in stereotyped pigmentation pattern along the lateral stripe of *nf1a/nf1b* mutants arise from failure of migration or differentiation of the regeneration and metamorphic melanophore lineages.
(A-F) Lateral stripe melanophores were initially imaged at 3 dpf in wild type (A) and *nf1a*$^{-/-}$*; nf1b*$^{-/-}$ (B) larvae, after which these animals were treated with 0.2 mM N-phenylthiourea (PTU) to prevent additional melanin synthesis. Therefore only the embryonic/ontogenetic melanophores melanized before PTU addition remain melanin-positive (C,D, embryonic/ontogenetic melanophores lettered) at 5 dpf. In contrast, the regeneration and metamorphic lineage of melanophores are melanin-negative and appear pale (C,D, red arrows). PTU removal after 5 dpf restores melanin synthesis, evident at 6 dpf when these melanophores become melanin-positive (E,F, black arrows). *nf1a/nf1b* mutants demonstrate gaps (F, brackets) in the pigmentation pattern along the lateral stripe when compared with wild type controls (E). Scale bars: 50 μm. (G) Tracking and quantification of lateral stripe melanophores in a 200 μm segment of the trunk in wild type (n=7) and *nf1a*$^{-/-}$*; nf1b*$^{-/-}$ (n=7) animals at 3 and 6 dpf.

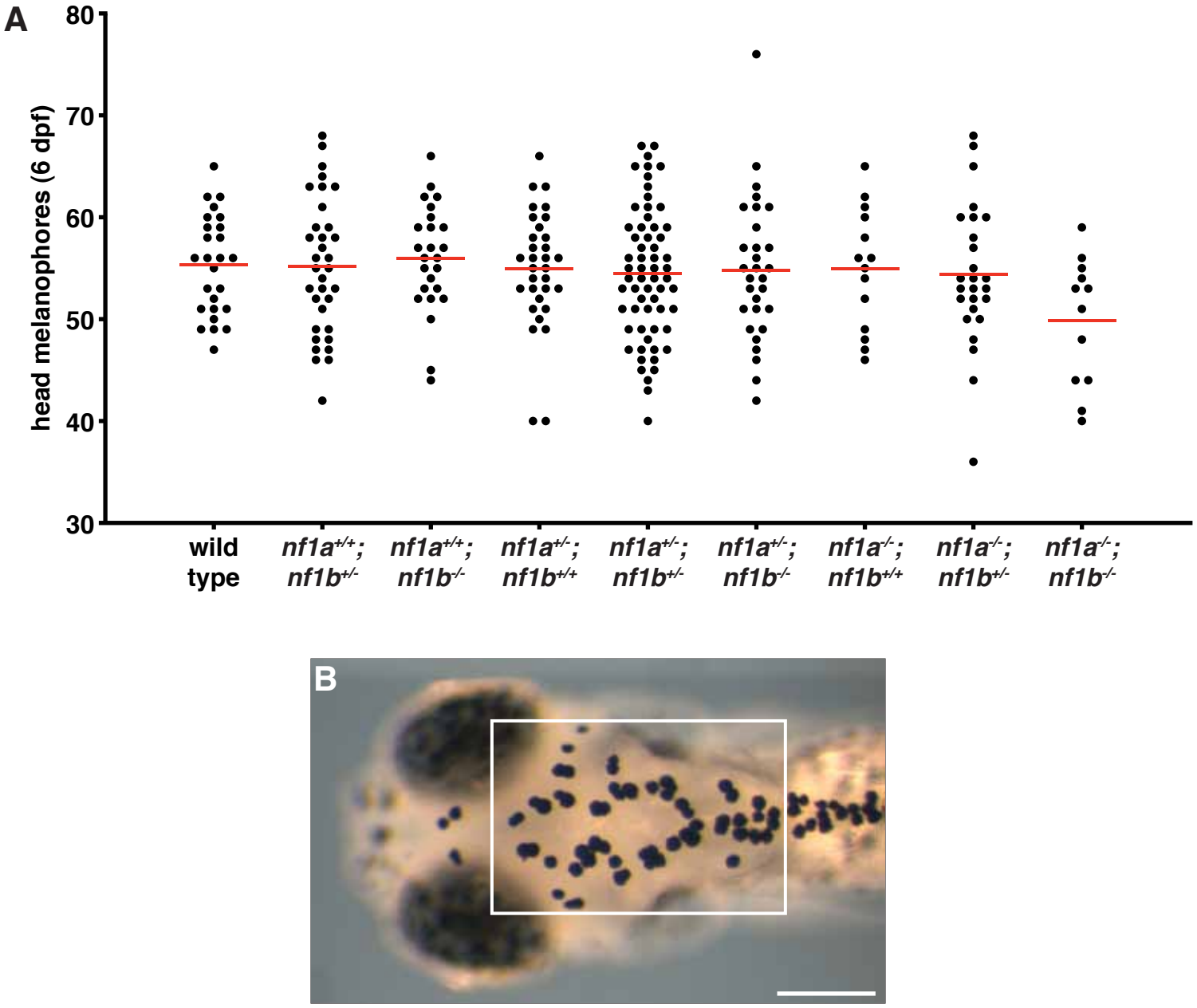

Fig. S14. Quantification of head melanophores in wild type and *nf1a*/*nf1b* mutant larvae at 6 dpf.
(A) Quantification of head melanophores from wild type (n=26), *nf1a*$^{+/+}$; *nf1b*$^{+/-}$ (n=34), *nf1a*$^{+/+}$; *nf1b*$^{-/-}$ (n=25), *nf1a*$^{+/-}$; *nf1b*$^{+/+}$ (n=32), *nf1a*$^{+/-}$; *nf1b*$^{+/-}$ (n=62), *nf1a*$^{+/-}$; *nf1b*$^{-/-}$ (n=30), *nf1a*$^{-/-}$; *nf1b*$^{+/+}$ (n=14), *nf1a*$^{-/-}$; *nf1b*$^{+/-}$ (n=26), and *nf1a*$^{-/-}$; *nf1b*$^{-/-}$ (n=12) larvae at 6 dpf. Each point represents the number of head melanophores in an individual embryo and red lines indicate mean values. (B) Representative image depicting head melanophores (boxed region) in a wild type larva at 6 dpf following epinephrine treatment and fixation. Scale bar: 200 μm.

Movie 1.

Movie 2.

Movie 3.